RSC Advances

ROYAL SOCIETY
OF CHEMISTRY

www.rsc.org/advances

Entrapping electrode materials within ultrathin carbon nanotube network for flexible thin film lithium ion batteries

Yang Wu, Hengcai Wu, Shu Luo, Ke Wang, Fei Zhao, Yang Wei, Peng Liu, Kaili Jiang, Jiaping Wang,[*] and Shoushan Fan

Department of Physics and Tsinghua-Foxconn Nanotechnology Research Center
Tsinghua University
Beijing, 100084, China
E-mail: jpwang@tsinghua.edu.cn

Abstract

A novel design of flexible thin film electrode for lithium ion batteries is reported. We employ ordered carbon nanotube (CNT) film, directly pulled from aligned CNT arrays, as a flexible skeleton. The functional electrode material is introduced by a one-step spray-painting approach. The electrode is self-sustained as a result of the strong interactions among CNTs. In such electrode configuration, the CNT network acts as micro electron pathways and its excellent mechanical property also ensures the flexibility. The electrodes fabricated in this way are electrochemically and mechanically superior in comparison with those prepared by the traditional slurry cast method. The full battery that contains $LiFePO_4$ cathode and $Li_4Ti_5O_{12}$ anode exhibits a high areal capacity over 200 μA h cm^{-2}, a stable output voltage of 1.82 V, an excellent reversibility, a high flexibility, and a light polarization in both flat and bent conditions. As a result, we suggest such electrodes with great promise for thin film lithium ion batteries to satisfy the energy storage demand in revolutionary portable electronics.

Introduction

The rapid growth of consumer electronic market boosts an explosive number of innovative designs for portable electronics.[1-3] The emergence of ultrathin and bendable smart electronics cannot be fulfilled until all components, for instance, the energy storage device, evolve into new configurations that are compatible with such revolutionary appearances.[4] Lithium ion battery (LIB) has dominantly powered portable electronics because of its high energy density, high power density, and long-term reliability.[5-7] The future generation portable electronics demand the battery to be seamlessly integrated into the system with limited space and thus trigger new challenges in the electrode design.[8-10] It is of great importance to develop a new scheme of LIBs that are highly portable, compact, and viable in versatile shapes.

In conventional LIBs, the battery electrode composed of an active material blended with a conductive agent and mechanically bound to metal foils by an organic binder. Typically, the metal foil and the organic binder weighed 25-30 % of the total mass of battery.[11,12] To improve the portability and reduce the thickness in the arrangement of thin film battery, it became necessarily meaningful to reduce these two electrochemically inactive components. One effective strategy was to devise novel synthetic routes that were able to directly integrate functional materials on carbonaceous material based conductive agents, e.g., carbon fiber, graphene, and carbon nanotube (CNT).[13,14,15] The direct growth/deposition of electrode materials decreased the necessity of organic binder and led to a great number of binder-free electrodes.[13-20] Furthermore, low dimensional carbonaceous materials were able to evolve into a 3D conductive network that served as conductive agent and current collector simultaneously.[21,22] Even though a large number of examples have been reported in recent

years, the obstacle still remained on how to effectively control the thickness of the electrode and interface newly developed methods to industry-level manufacturing.

The direct usage of commercial battery material would accelerate the shift of manufacturing from classical batteries to thin film batteries for emerging portable electronics. Herein, we directly utilized the commercial $LiFePO_4$ (LFP) and $Li_4Ti_5O_{12}$ (LTO) powders as the active material to fabricate electrodes for thin film LIBs. CNT film, simply drawn from super-aligned CNT arrays, was employed as the conducting agent.[23] The enthusiasm of such choice was originally from the remarkable electrical and mechanical properties of CNTs.[24,25] Indeed, these slender CNT films were consisted of continuous CNTs yarns with diameters of 40-50 nm arranged in a parallel fashion, an ideal precursor for constructing an ultrathin conductive network in the electrode without any interruption. We utilized a spray-painting technique, which had shown a great range of applications in forming depositions on various substrates, to fabricate electrodes.[26] The electrode structure comprised alternated CNT layer and electrode material layer. As the ethanol as the spray medium evaporized, the composite electrode strengthened itself by the strong interaction among CNTs. As a matter of fact, electrode materials were tightly confined in such CNT network. Thus, these electrodes were free of organic binders and metal foils and held great potential to meet the critical requirement in volume for future portable electronics.

Experimental

Electrode Preparation

$LiFePO_4$ (Tianjiao Chemical co., Shenzhen, China) and $Li_4Ti_5O_{12}$ (Reshine, China) powders were used as purchased. 1000 mg LFP (LTO) powder was loaded in 100 mL ethanol. By 30 minutes ultrasonication in a tip-sonicator, the powder was dispersed. The suspension was then immediately transferred into a painter for the subsequent spray-painting process. CNT

films, directly drawn from super-aligned CNT array grown on an 8-inch Si wafer, were crossly stacked on a 3.5 cm × 3.5 cm Teflon square frame and used as the substrate. Details for preparing CNT films could be found in early publications.[23] LFP or LTO powders were then sprayed on cross-stacked CNT film with a gentle nitrogen flow. Each spray-painting step took 2 minutes for LTO and 4 minutes for LFP, and consumed 10 mL of the suspension. The dependence of painting time and mass loading was shown in Fig. S1a. Between each spray-painting, the sample was covered with a cross-stacked CNT film and, in the meantime, the suspension was ultrasonicated for another 2 minutes to keep the powder from precipitation. This process was repeated for 5 times and finished off by placing another cross-stacked CNT film on the top. Photographs of thin film electrodes were shown in Fig. S1. Classical electrodes were prepared by mixing LFP and LTO powders with Super P and PVDF at a weight ratio of 8:1:1 in N-methylpyrrolidone (NMP) as control samples. The resulted slurry was cast on Al or Cu films and dried in a vacuum oven at 120 $^{\circ}$C for overnight.

Morphological, mechanical, and electrochemical characterization

The microstructure of LFP/CNT and LTO/CNT was observed in a scanning electron microscope (FEI, Sirion 200, 10 kV) and a transmission electron microscope (FEI, Tecnai G2F20, 200 kV). Tensile tests were carried out on an Instron 5848 microtester with a strain rate of 5% min^{-1}. The tensile direction was in 0° and 90° to the cross-stacked CNTs for LFP/CNT and LTO/CNT electrodes. Classical LFP and LTO electrodes were peeled off directly from metal foils for tensile test. Half-cell samples were assembled in a dry-argon filled glove-box (M. Braun inert gas systems Co. Ltd.) in accordance with 2016 arrangement using Li foil as the counter electrode and 1M LiPF$_6$ in an EC/DEC (1:1 v/v) mixture as the electrolyte. Galvanostatic tests were carried out in 2.5 – 4.2 V for LFP and 1.0 – 2.5 V for LTO on a Land battery tester (Wuhan Land Electronic Co., China). CV measurements were

performed on a potentiostat/galvanostat instrument with the same voltage range (Princeton PARStat 2273). Scan rates were 0.2 mV s^{-1} and 0.5 mV s^{-1} for each type of electrode. The CV profiles of full battery were also collected in 2016 arrangement with a voltage range of 1.0 – 2.5 V at scan rates of 0.2 mV s^{-1}, 0.5 mV s^{-1}, and 1 mV s^{-1}.

Full battery preparation

The full battery was prepared by choosing LFP/CNT as cathode and LTO/CNT as anode. The film electrode was cut into 3 cm × 3 cm squares from the Teflon frame with an infrared laser. The slim electrode was carefully folded twice and placed on a 1.5 cm-wide CNT buckypaper strip. Ethanol was used to densify and stick the slim electrode on the CNT buckypaper. A slight amount of 10 wt% PVDF in NMP was applied on the surface of the electrode to glue it with the Celgard 2400 separator. Ni slabs, equipped with a heat sensitive tape, were point-welded with CNT buckypaper. The Ni slab ensured an airtight sealing with Al laminated foil and acted as positive and negative poles for the battery. The Al foil package was finally sealed inside the glove box, in which a few drops of LiPF$_6$ electrolyte were added. The battery was kept still for 12 hours before electrochemical tests carried out on the Land system.

Results and discussion

Sample morphology and microstructure

The spray-on fabrication process was illustrated in Fig. 1a. The prerequisite of the spray-painting approach was to make suspensions of LFP and LTO, which were implemented by dispersing the powder in ethanol with tip-ultrasonication for 30 minutes. Subsequently, the as-prepared suspension was loaded in a nebulizer and sprayed on a cross-stacked CNT film served as a substrate under a nitrogen flow. Another layer of cross-stacked CNT film was coated on the top and the suspension was sprayed again. Thus, the total thickness of an

electrode was easily tuned by varying the times of repeating such process. In this article, the spray-painting process was carried out for five times for an LFP/CNT or LTO/CNT electrode with an average thickness of 10 μm. With painting time of 4 minutes and 2 minutes for each layer of LFP and LTO, respectively, the mass ratio of CNT in such thin electrodes was less than 5% by using the areal density of 2 μg cm^{-2} for a single-layered CNT film (Fig. S1). [27]

The microstructure of both LFP/CNT and LTO/CNT was investigated by scanning electron microscopy (SEM) and transmission electron microscopy (TEM). Both top view and cross-sectional images revealed similar morphology of all electrodes (Fig. 1b to 1e). A cross-sectional SEM image of an LFP/CNT sample suggested that typical electrodes resembled a lasagna-like structure in which LFP layers alternated with CNT layers (*cf.* Fig. 1b). The top view microstructure was exemplified by an LFP/CNT sample in Figure 1c and 1d. Flexible CNT film blanket covered the whole layer of LFP. The contact of LFP with CNT was established, even though the diameter distribution for commercial powders was quite wide. It is worth to note that spray-painted particles did not occupy the CNT film completely but left a great deal of empty voids where CNT yarns were able to connect with those from adjacent layers (*cf.* white circles in Fig. 1c). The evaporation of ethanol led to the densification CNT yarns, and due to the lateral van der Waals interactions, this process was not reversible. Indeed, the abovementioned interactions were so strong that raw CNTs yarns processed with an ethanol shrinking approach have exhibited excellent mechanical properties.[28] In this case, ethanol evaporation induced such inter-layer van der Waals interactions, and, as a matter of fact, the fluffy CNT film was turned into a compact structure. The electrode was freestanding by the mechanical support from CNTs. This step also greatly decreased the thickness of electrodes. Consequently, LFP/LTO particles were confined in such CNT films, which functioned in two aspects, a conductive network and a flexible but

firm structural scaffold. The electrode did not need any binders and was integrated with current collectors that composed of CNT yarns. Further morphological information could be viewed in Fig. S2.

The performance of the electrode was fundamentally determined by its microstructure. Commonly, the electrochemical limitation lay in two aspects, the electronic transfer and the ionic transfer. With respect to the active material in this electrode configuration, the electronic transfer was obviously facilitated by those CNT yarns that approached particles from all directions. Fig. 1e revealed that particles with typical sizes in commercial powders were grabbed by a large amount of CNT yarns. Embedding with guest particles will not hamper the electrical property of such CNT yarns.[29] In fact, these yarns were important micro pathways for electrons to reduce the internal resistance. According to a previous study, the conductivity was isotropic for cross-stacked CNT films.[30] The electrons can be equally delivered from horizontal and vertical directions, as shown in Fig.1e. This isotropic conductive network held particular importance to alleviate the issue of polarization. As to the ionic transfer in this type of electrode, the CNT network, made from crossly stacking ordered CNT films, explicitly possessed a significant deal of pores with a variety of diameters (Fig. 1b, 1c, and 1e). This feature had little battier to the wetting by electrolyte. Therefore, the electrode design by entrapping commercial LFP and LTO powders within CNT films should benefit both electron and ion transfers. We expected each layer in such lasagna-like electrode to exhibit the same electrochemical property because of the similar structure and the same fabrication process.

Electrochemical and mechanical characterizations

To evaluate the merit as electrode of thin film LIBs, galvanostatic characterizations were carried out to investigate the specific capacity of LFP/CNT and LTO/CNT. These tests were

performed in a 2016 half-cell arrangement using Li foils as the counter electrode. For comparison, LFP and LTO slurries, made by mixing LFP or LTO powder, super P, and polyvinylidene fluoride (PVDF) at a weight ratio of 8:1:1, were also prepared. The slurry was casted on metal current collectors to make control samples. As shown in Fig. 2a and 2b, 0.1 C test revealed 150 and 151 mA h g^{-1} specific capacities of LFP/CNT and LTO/CNT electrodes, respectively, at 10th cycle. (Here 1/n C denoted that n hours were required to charge or discharge the electrode to its nominal specific capacity). Although both values were lower than those at fully charged/discharged states in theory, they all exhibit good reversibility for 50 cycles and no obvious capacity decay was recorded. The remarkable capacity retention of LFP/CNT and LTO/CNT electrodes was indicative of the excellent mechanical property resulting from the robust CNT network. In contrast, electrodes made from the slurry cast method delivered lower specific capacities, 131 mA h g^{-1} for LFP and 134 mA h g^{-1} for LTO, at 0.1 C rate. In addition, classical LFP electrodes showed fast capacity decay in 50 cycles. For the rate test, the specific capacities of either LFP/CNT or LTO/CNT were higher than those of classical LFP or LTO electrodes at all rates, reflecting the efficient ion and electron transport in the CNT network (Fig. 2c and 2d). The different electrode material led to the difference in the rate performance. The specific capacity decreased when the current density increased for all kinds of LFP electrodes. In contrast, both LTO/CNT and classical LTO electrodes revealed almost constant specific capacities at various rates up to 5 C (*cf.* Fig. 2d). This behavior can be ascribed to the high ionic conductivity of LTO, which had been exploited in ultrahigh-rate energy storage devices.[31,32] The cycle and rate tests suggested the superiority in the lasagna-like electrode structure, which could be ascribed to the advantage in optimized electron and ion transfers. Another reason could arise from the mechanical property of the CNT network. According to the tensile test results (Fig. 3), LFP/CNT and LTO/CNT electrodes provided tensile strengths of

2.49 MPa and 2.16 MPa, respectively, whereas classical LFP and LTO electrodes fractured at 0.25 MPa and 0.12 MPa, respectively.

Cyclic voltammetry (CV) provided further information for LFP/CNT and LTO/CNT electrodes. Fig. 4a and 4b compiled CV profiles recorded at 0.2 mV s^{-1} scan rate. The cathodic and anodic peaks, corresponding to lithiation and delithiation processes, occurred at 3.25 and 3.65 V for LFP/CNT, and at 1.43 and 1.75 V for LTO/CNT, respectively. No additional cathodic or anodic peaks were observed besides the characteristic signals corresponding to electrochemical reactions with Li$^+$ of these well-known materials. This observation also proved that CNT itself did not involve any electrochemical process but only acted as a spectator component in such voltage range. CV profiles of classical LFP and LTO electrodes that made from the slurry cast method were also plotted in Fig. 4 to make a comparison. It is clear that electrodes prepared by this traditional method exhibited a similar electrochemical behavior, however, the separation between cathodic and anodic peaks increased and was further pronounced when the scan rate increased to 0.5 mV s^{-1} (Fig. S3). The separation between cathodic and anodic peaks indicated the extent of polarization, which usually resulted in energy loss due to the hysteresis in each charging/discharging cycle. By entrapping powders of active materials inside cross-stacked CNT network, the polarization issue has been properly addressed and this is of great importance for practical applications of batteries.

Full battery evaluation

The full battery was also assembled to probe the viability of this lasagna-like electrode in thin film batteries. In this full-cell assembly, LFP/CNT acted as cathode while LTO/CNT was anode. Celgard 2400 separator and electrolyte of 1 M LiPF$_6$ in ethylene carbonate (EC) and diethyl carbonate (DEC) (1:1) were used. To fabricate full-cell batteries, such LFP/CNT

and LTO/CNT electrodes were folded into squares with a length of 1.5 cm and then placed on CNT buckypaper strips with a size of 3 cm × 1.5 cm. The CNT buckypaper was 40 μm thick and composed of hundreds of CNT films aligned in the same direction. By gently dropping ethanol, the electrodes were densified and firmly attached to CNT buckypaper without application of any glue. The CNT buckypaper showed a sheet resistance as low as 5 Ω sq^{-1}. Cross-sectional SEM image revealed that the total thickness of the full-cell assembly was around 100 μm, including the polymer separator and CNT buckypaper strips. Noticeably, this value was no thicker than carbon conductive tape (Fig. 5a, 5b, and S4). The galvanostatic characterizations were carried out at an areal current density of 100 μA cm^{-2} and the charge/discharge voltage profiles were shown in Fig. 5c. The narrow gap between voltage plateaus at 1.90 and 1.82 V was implicit of light polarization, which can be attributed to the effective ionic and electronic pathways established by the CNT network. The cell potential at 1.82 V was in good agreement with the electromotive force of LFP and LTO occurred at 3.4 and 1.5 V, vs Li$^+$/Li, respectively. [33-35] Thus, this output is quite reasonable and is demonstrated by powering a red LED bulb (Fig. 5d). An illuminating LED plugged on a bent battery in Figure 5e indicated that this assembly was eligible to work under different circumstances where unconventional shapes or flexible structures were demanded. This also demonstrated the mechanical robustness of these thin film electrodes that resulted from the CNT network.

The cyclic stability was assessed by long-term galvanostatic cycles. At an areal current density of 100 μA cm^{-2}, this thin-film battery can deliver 220 μAh cm^{-2} at 10th cycle, corresponding to 65 mAh g^{-1} based on the total mass of electrodes and the separator (Fig. 5f). The areal capacity decreased to 202 μAh cm^{-2} after 30 cycles, corresponding to 91% capacity retention. The columbic efficiency was maintained above 97% throughout the measurement. When the current density increased to 1000 μA cm^{-2}, the areal capacity

decreased to 130 µAh cm^{-2}. Since little capacity fading was monitored in the half-cell rate test of LTO/CNT electrode, we postulate that LFP cathode played as a rate-limiting factor in the full battery. The capacity retention was also remarkable in high areal current density measurements. In Fig. 5g, the full battery still delivered a reversible capacity of 125 µAh cm^{-2} after 50 cycles at an areal current density of 1000 µA cm^{-2}, corresponding to a capacity retention of 96%. CV tests at scan rates ranging from 0.2 mV s^{-1} to 1 mV s^{-1} verified the cyclic stability at high current densities (Fig. S5). The results of electrochemical characterizations suggested that the CNT network was capable to hold LFP and LTO powders. Under bent conditions, the full battery sample revealed almost the same performance. A sample bent by 180° was still able to deliver over 200 µAh cm^{-2} (Fig. S6). SEM images revealed similar microstructures for a bent battery after cycle tests in comparison with as-prepared samples (*cf.* Fig. S7 & Fig. 1). More importantly, no powder fall-off was observed according to post-cycle SEM observation. Therefore, the lasagna-like electrode showed great viability under various mechanical deformations and maintained its mechanical and electrochemical properties.

All above-mentioned areal specific capacities were presented by samples that contained only one cell. The fabrication process that took advantage of the spray-painting technique was very easy to scale-up, and was able to offer stable quality of the electrodes. As a matter of fact, multiple cells can be prepared in batch. To increase the areal density, three LFP/LTO cells were connected in parallel and sealed in the same way. Specific capacity around three times (650 µA h cm^{-2} vs. 220 µA h cm^{-2}) that of a single LFP/LTO cell was delivered under a current density of 1000 µA cm^{-2} (Fig S8). Accordingly, this thin-film approach is capable to satisfy a large variety of battery modules for high capacity (in parallel) or high voltage (in serial) applications but in the same time with little volume occupation.

Conclusions

In conclusion, we have demonstrated fabrication of LFP/CNT and LTO/CNT thin-film electrodes with tunability in thickness to address the challenge in energy storage for next-generation portable electronics. Functional electrode materials are successfully confined in an isotropic 3D conductive network and immobilized by cross-linked CNTs due to the strong van der Waals interactions. Therefore, the total volume of the electrode is reduced by the removal of binders and metal current collectors. The full battery delivers a reversible areal capacity over 200 μA h cm^{-2}, which corroborates superior ion and electron transfers in such lasagna-like electrodes design. The CNT scaffold also guarantees the stable capacity delivery under high current densities and the viability of thin film electrodes under mechanical deformations. The compactness for the whole battery suggests great promise in satisfying critical requirement of space in ultra portable electronics. Finally, the strategy of electrode design in this work suggests a new platform that is available for making a rich variety of flexible thin film batteries. The process of fabrication is potentially scalable since it uses commercial electrode materials and only involves a one-step spray-painting in low-cost and low-toxic ethanol.

Notes and references

1   J. A. Rogers, Z. Bao, K. Baldwin, A. Dodabalapur, B. Crone, V. R. Raju, V. Kuck, H. Katz, K. Amundson, J. Ewing and P. Drzaic, *Proc. Natl. Acad. Sci.,* 2001, **98**, 4835.

2   C. Wang, D. Hwang, Z. Yu, K. Takei, J. Park, T. Chen, B. Ma and A. Javey, *Nat. Mater.,* 2013, **12**, 899.

3   A. Nathan, A. Ahnood, M. T. Cole, S. Lee, Y. Suzuki, P. Hiralal, F. Bonaccorso, T. Hasan, L. Garcia-Gancedo, A. Dyadyusha, S. Haque, P. Andrew, S. Hofmann, J. Moultrie, D. Chu, A. J. Flewitt, A. C. Ferrari, M. J. Kelly, J. Robertson, G. Amaratunga and W. I. Milne, *Proc. IEEE,* 2012, **100**, 1486.

4   H. Li, Q. Zhao, W. Wang, H. Dong, D. Xu, G. Zou, H. Duan and D. Yu, *Nano Lett.,* 2013, **13**, 1271.

5   M. Armand and J. M. Tarascon, *Nature,* 2008, **451**, 652.

6   B. Scrosati and J. Garche, *J. Power Sources,* 2010, **195**, 2419.

7   J. M. Tarascon and M. Armand, *Nature,* 2001, **414**, 359.

9   M. Koo, K. I. Park, S. H. Lee, M. Suh, D. Y. Jeon, J. W. Choi, K. Kang and K. J. Lee, *Nano Lett.,* 2012, **12**, 4810.

9   J. B. Bates, N. J. Dudney, D. C. Lubben, G. R. Gruzalski, B. S. Kwak, X. Yu and R. A. Zuhr, *J. Power Sources,* 1995, **54**, 58.

10 Y. H. Kwon, S. W. Woo, H. R. Jung, H. K. Yu, K. Kim, B. H. Oh, S. Ahn, S. Y. Lee, S. W. Song, J. Cho, H. C. Shin and J. Y. Kim, *Adv. Mater.,* 2012, **24**, 5192.

11 L. Hu, J. W. Choi, Y. Yang, S. Jeong, F. La Mantia, L. F. Cui and Y. Cui, *Proc. Natl. Acad. Sci.,* 2009, **106**, 21490.

12 G. Zhou, F. Li and H. M. Cheng, *Energy Environ. Sci.,* 2014, **7**, 1307.

13 O. Toprakci, H. A. K. Toprakci, L. Ji, G. Xu, Z. Lin and X. Zhang, *ACS Appl. Mater. Interfaces,* 2012, **4**, 1273.

14 H. Wolf, Z. Pajkic, T. Gerdes, M. Willert-Porada, *Journal of Power Sources*, 2009, **190**, 157.

15 Z. S. Wu, G. Zhou, L. C. Yin, W. Ren, F. Li, H. M. Cheng, *Nano Energy,* 2012, **1**, 107.

16 X. Jia, C. Yan, Z. Chen, R. Wang, Q. Zhang, L. Guo, F. Wei and Y. Lu, *Chem. Commun.,* 2011, **47**, 9669.

17 X. Li, J. Yang, Y. Hu, J. Wang, Y. Li, M. Cai, R. Li and X. Sun, *J. Mater. Chem.,* 2012, **22**, 18847.

18 H. X. Zhang, C. Feng, Y. C. Zhai, K. L. Jiang, Q. Q. Li and S. S. Fan, *Adv. Mater.,* 2009, **21**, 2299.

19 Y. Wu, Y. Wei, J. P. Wang, K. L. Jiang and S. S. Fan, *Nano Lett.,* 2014, **13**, 818.

20 K. Fu, O. Yildiz, H. Bhanushali, Y. Wang, K. Stano, L. Xue, X. Zhang and P. D. Bradford, *Adv. Mater.,* 2013, **25**, 5109.

21 C. Ban, Z. Wu, D. T. Gillaspie, L. Chen, Y. Yan, J. L. Blackburn and A. C. Dillon, *Adv. Mater.,* 2010, **22**, E145.

22 S. Luo, K. Wang, J. P. Wang, K. L. Jiang, Q. Q. Li and S. S. Fan, *Adv. Mater.,* 2012, **24**, 2294.

23 K. L. Jiang, Q. Q. Li and S. S. Fan, *Nature,* 2002, **419**, 801.

24 M. Zhang, S. Fang, A. A. Zakhidov, S. B. Lee, A. E. Aliev, C. D. Williams, K. R. Atkinson and R. H. Baughman, *Science,* 2005, **309**, 1215.

25 X. B. Zhang, K. L. Jiang, C. Feng, P. Liu, L. N. Zhang, J. Kong, T. Zhang, Q. Q. Li and S. S. Fan, *Adv. Mater.,* 2006, **18**, 1505.

26 N. Singh, C. Galande, A. Miranda, A. Mathkar, W. Gao, A. L. M. Reddy, A. Vlad and P. M. Ajayan, *Sci. Rep.,* 2012, **2**, 481.

27 K. L. Jiang, J. P. Wang, Q. Q. Li, L. Liu, C. H. Liu and S. S. Fan, *Adv. Mater.,* 2011, **23**, 1154.

28 K. Liu, Y. H. Sun, R. F. Zhou, H. Zhu, J. P. Wang, L. Liu, S. S. Fan and K. L. Jiang, *Nanotechnology* 2010, **21**, 045708.

29 M. D. Lima, S. Fang, X. Lepró, C. Lewis, R. Ovalle-Robles, J. Carretero-González, E. Castillo-Martínez, M. E. Kozlov, J. Oh, N. Rawat, C. S. Haines, M. H. Haque, V. Aare, S. Stoughton, A. A. Zakhidov and R. H. Baughman, *Science,* 2011, **331**, 51.

30 K. Liu, Y. Sun, P. Liu, X. Lin, S. Fan and K. Jiang, *Adv. Funct. Mater.* 2011, **21**, 2721.

31 K. Naoi, W. Naoi, S. Aoyagi, J. Miyamoto and T. Kamino, *Acc. Chem. Res.,* 2013, **46**, 1075.

32 S. Chen, Y. Xin, Y. Zhou, Y. Ma, H. Zhou and L. Qi, *Energy Environ. Sci.,* 2014, DOI: 10.1039/C3EE42646G

33 A. K. Padhi, *J. Electrochem. Soc.,* 1997, **144**, 1188.

34 K. Zaghib, M. Simoneau, M. Armand and M. Gauthier, *J. Power Sources,* 1999, **81**, 300.

35 E. Ferg, R. J. Gummow, A. de Kock and M. M. Thackeray, *J. Electrochem. Soc.,* 1994, **141**, L147.
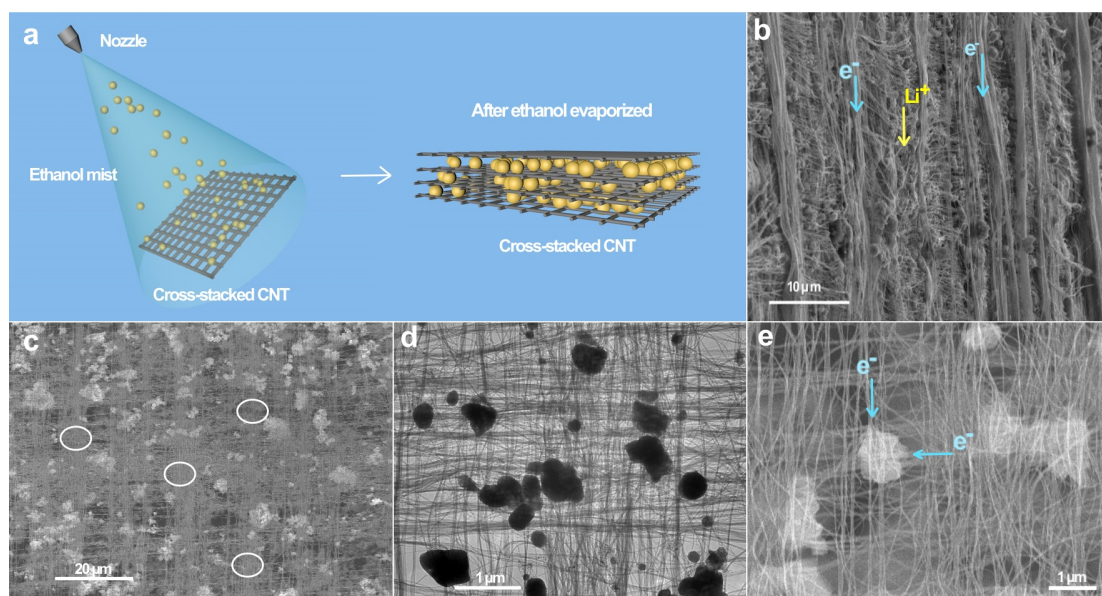
Fig. 1 (a) Schematic illustration of LFP/CNT and LTO/CNT thin film electrode fabrication by spray-painting. (b) Typical cross-sectional SEM image of an LFP/CNT electrode revealed a lasagna-like microstructure. The sample was folded twice and placed on a CNT buckypaper. Cyan and yellow arrows indicated possible electron and ion paths. (c) Typical top view SEM image of an LFP/CNT electrode. White circles hinted possible regions where inter-layer CNTs cross-linked. (d) TEM image of a single-layer LFP/CNT. (e) SEM top view image at high magnification showed LFP particles confined in the CNT network. The conductivity was isotropic. Possible pathways of electron delivery were indicated with cyan arrows.
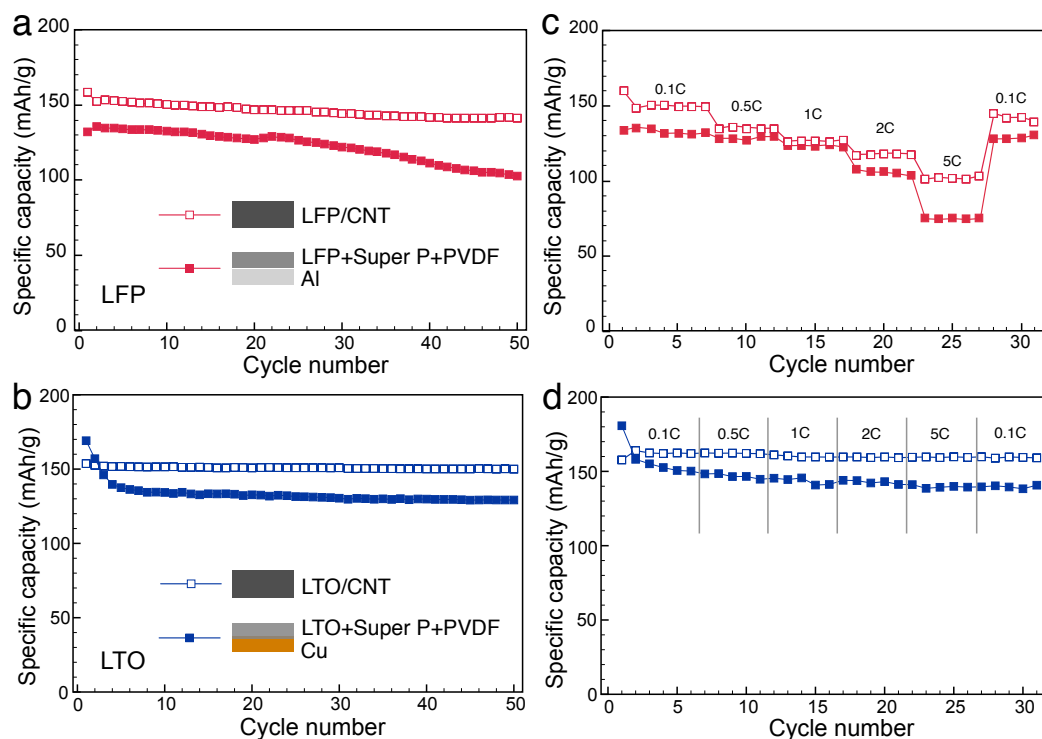
Fig. 2 Electrochemical characterizations carried out in half-cell arrangement for LFP/CNT and LTO/CNT electrodes. (a) & (b) Galvanostatic measurements of LFP/CNT and LTO/CNT at 0.1 C rate. (c) & (d) Rate performance measurements up to 5 C rate. All results were compared with classical LFP or LTO electrodes prepared by the slurry cast method.
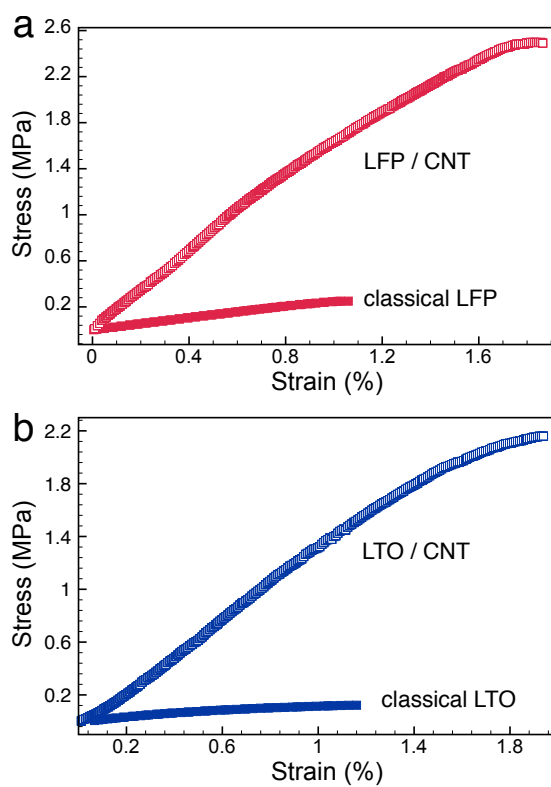
Fig. 3 Stress-strain curves of (a) LFP/CNT and classical LFP electrodes, and (b) LTO/CNT and classical LTO electrodes.
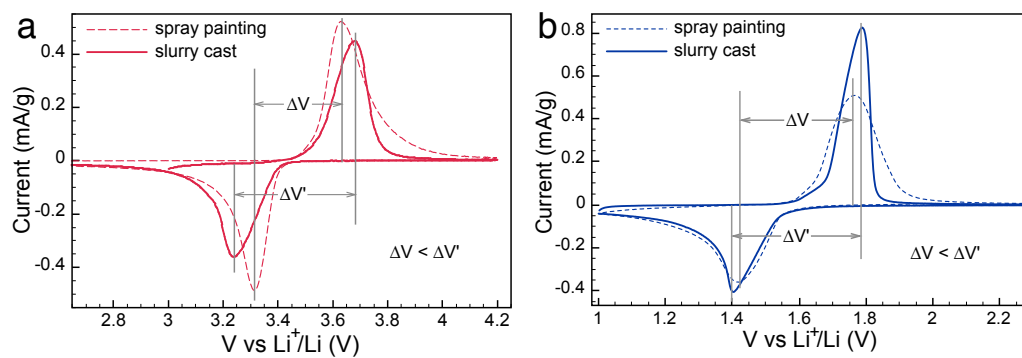
Fig. 4 CV profiles of LFP/CNT (a) and LTO/CNT (b) at 0.2 mV s^{-1} scan rate, respectively. The smaller separation between cathodic and anodic peaks suggested a low degree of polarization and faster kinetics in LFP/CNT and LTO/CNT electrodes.
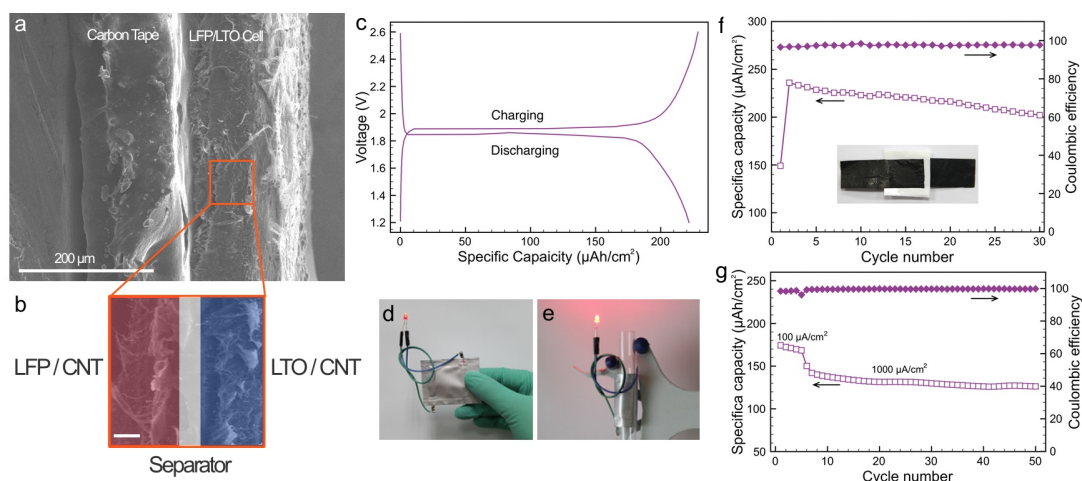
Fig. 5 (a) & (b) Side views of an LFP/LTO battery in SEM. The entire thickness of the battery was not greater than carbon conductive tape, which is placed in parallel to the sample in (a). The scale bar in (b) corresponded to 20 μm. (c) Voltage profiles of a charging/discharging process for a full battery between 1.2 to 2.6 V. Charged LFP/LTO batteries powered red LED in flat (d) and bent condition (e). The battery in (e) was mounted on a 10-mm test tube. (f) Galvanostatic measurements at 100 μA cm^{-2} current density. Inset: photograph of a sample before packaged. (g) Measurements at 1000 μA cm^{-2} current density for both charging and discharging. Coulombic efficiencies were plotted as solid rhomboids in (f) and (g).

Supplementary Information

Entrapping electrode materials within ultrathin carbon nanotube network for flexible thin film lithium ion batteries

Yang Wu, Hengcai Wu, Shu Luo, Ke Wang, Fei Zhao, Yang Wei, Peng Liu, Kaili Jiang, Jiaping Wang,[*] and Shoushan Fan

Estimation of CNT wt% in the thin film electrode:

LFP or LTO powders were spray-painted on a 1×1 cross-stacked CNT film and this procedure was repeated for 5 times to make each sample. Another 1×1 CNT film covered the top surface. Thus, each electrode contained 12 (2×6) single-layer CNT films. The size of each sample was 3 cm × 3 cm, equal to a total area of 9 cm^2. The areal density of single-layered CNT film was 0.002 mg cm^{-2} according to Ref. 1. Thus, the mass of CNT in each sample could be calculated as 0.216 mg. In this work, total spray-painting time for LFP/CNT and LTO/CNT was 20 minutes and 10 minutes, respectively. These conditions resulted in an average mass of 4.62 mg for LFP/CNT and 4.68 mg for LTO/CNT (cf. Fig. S1a). Therefore, CNT wt% for LFP/CNT and LTO/CNT was 4.62 % and 4.67 %, respectively.
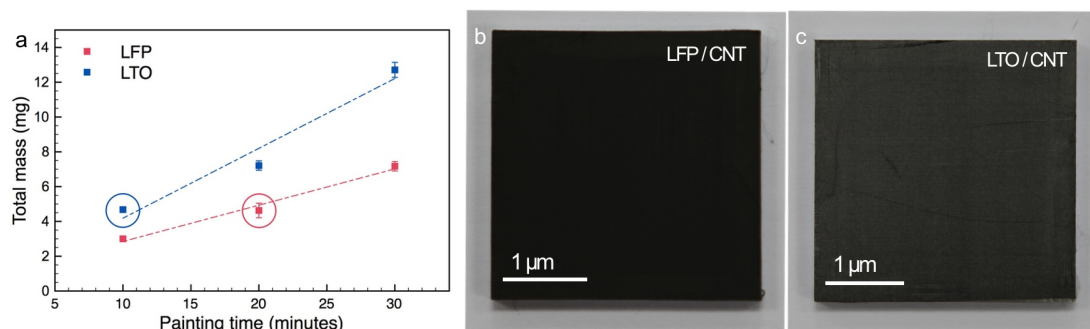

Fig. S1 (a) Dependence of total mass loading of LFP or LTO powders in CNT films on painting time. (b) & (c) Photographs of LFP/CNT and LTO/CNT samples, which are suspended on square Teflon frames, prepared at conditions circled in (a).
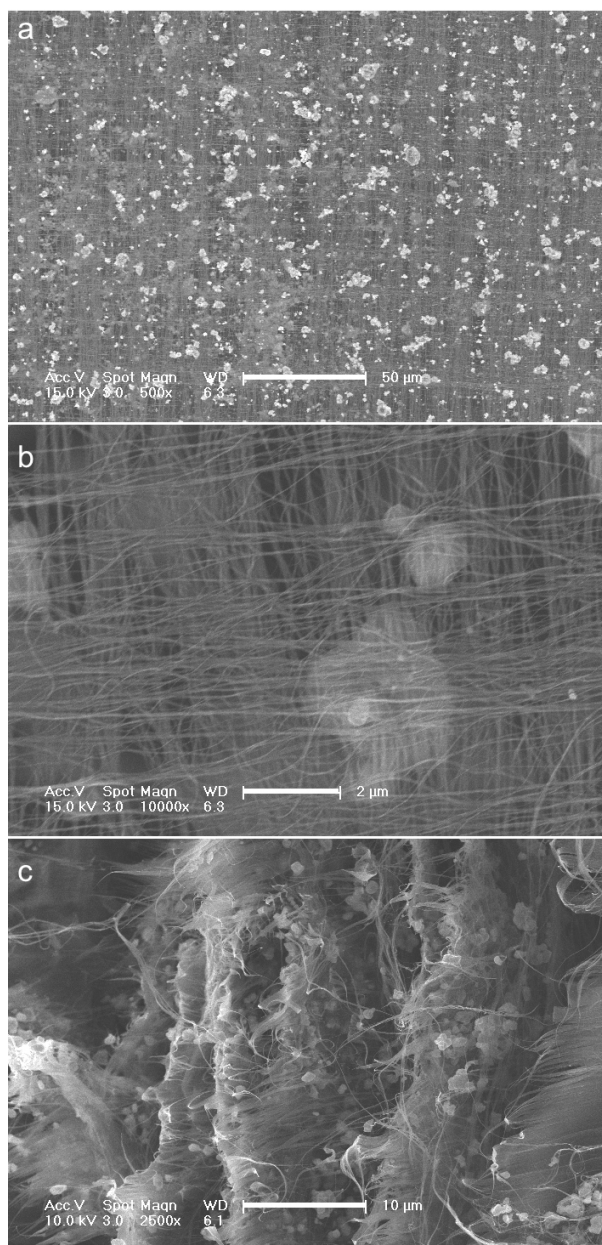
Fig. S2 SEM images of thin film electrodes prepared with the spray painting method. (a) & (b) Top view of LTO/CNT electrode in high and low magnifications, respectively. LTO particles were embedded in the CNT film and entrapped by a bunch of CNT yarns (b). (c) Cross-sectional SEM image. The sample was cut by a razor.
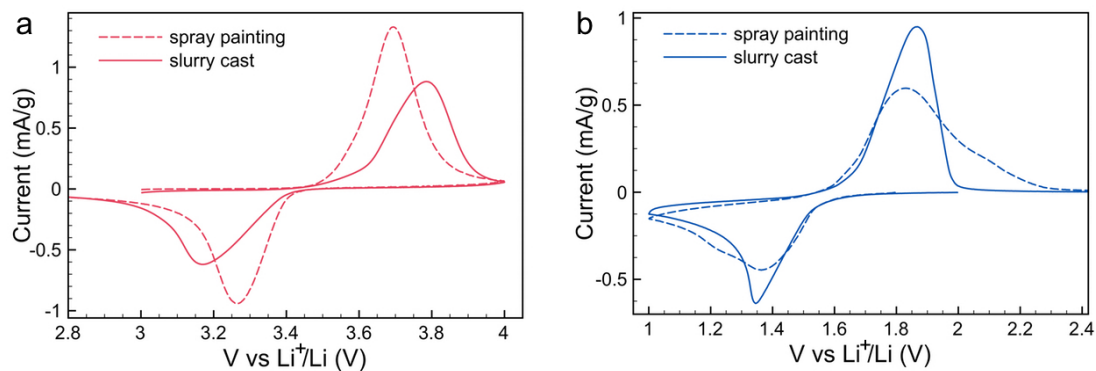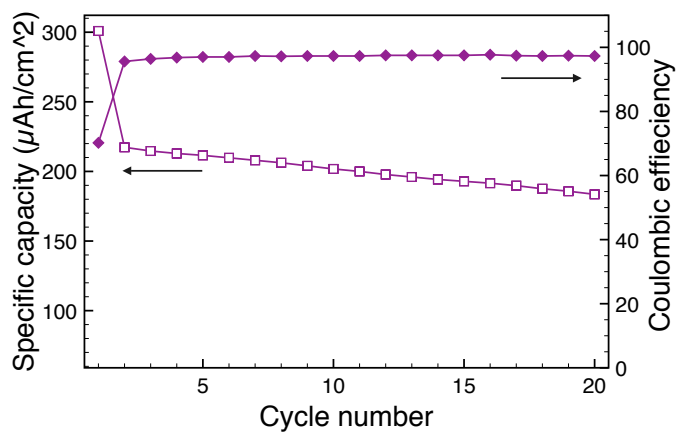
Fig. S3 CV profiles of (a) LFP/CNT and (b) LTO/CNT at 0.5 mV s^{-1} scan rate.
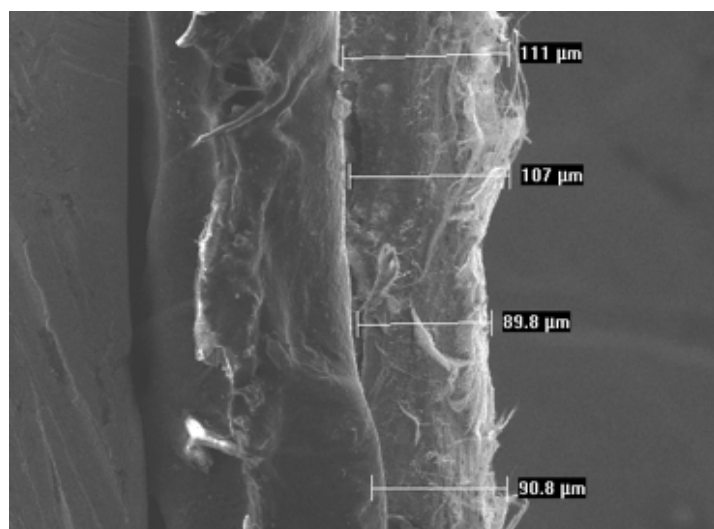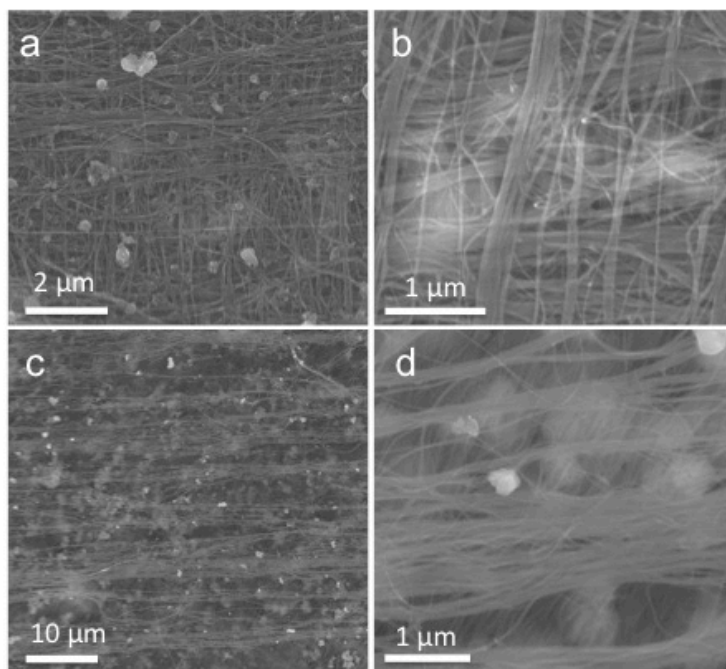

Fig. S4 Thickness of an LFP/LTO thin film battery measured in cross-sectional SEM image. The carbon tape was presented on the left as a reference.
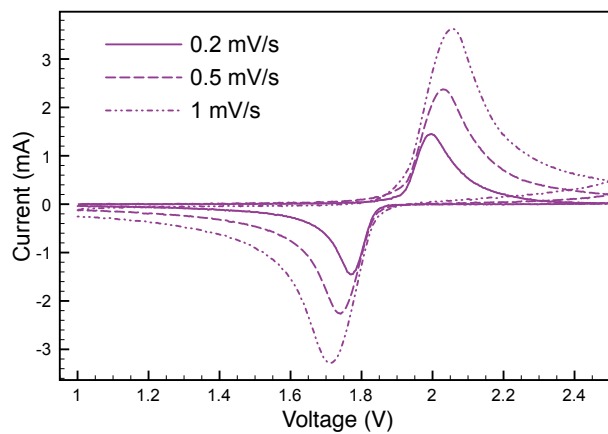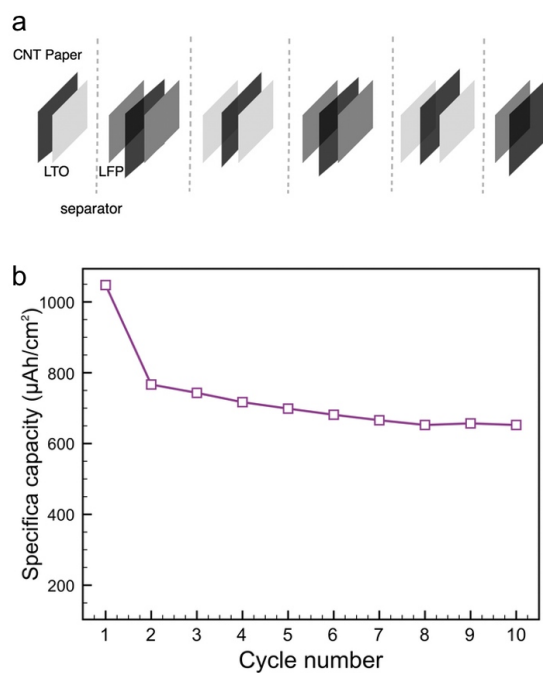
Fig. S5 CV profiles of LFP/LTO full battery prepared with the spray-painting method at various scan rates.

Fig. S6 Cycle performance measured at 100 µA cm^{-2} current density for a 180° bent battery.

Fig. S7 Post-cycle microstructure images by SEM for LFP/CNT (a and b) and LTO/CNT (c and d) electrodes.

Fig. S8 (a) Illustration of connecting 3 LFP/LTO batteries in parallel. The parallel configuration was arranged by point-welding Ni tab (not drawn) to all CNT papers attached to LFP electrodes for the positive pole, and to those attached to LTO electrodes for the negative pole. (b) Areal specific capacity measured at 1000 μA cm^{-2}.

1 K. L. Jiang, J. P. Wang, Q. Q. Li, L. Liu, C. H. Liu and S. S. Fan, *Adv. Mater.,* 2011, **23**, 1154